High-Fidelity Preservation of Quantum Information During Trapped-Ion Transport

Peter Kaufmann, Timm F. Gloger, Delia Kaufmann, Michael Johanning, and Christof Wunderlich*
Department Physik, Naturwissenschaftlich-Technische Fakultät, Universität Siegen, 57068 Siegen, Germany

(Received 5 April 2017; published 2 January 2018)

A promising scheme for building scalable quantum simulators and computers is the synthesis of a scalable system using interconnected subsystems. A prerequisite for this approach is the ability to faithfully transfer quantum information between subsystems. With trapped atomic ions, this can be realized by transporting ions with quantum information encoded into their internal states. Here, we measure with high precision the fidelity of quantum information encoded into hyperfine states of a $^{171}Yb^{+}$ ion during ion transport in a microstructured Paul trap. Ramsey spectroscopy of the ion's internal state is interleaved with up to 4000 transport operations over a distance of 280 μm each taking 12.8 μs. We obtain a state fidelity of $99.9994(^{+6}_{-7})\%$ per ion transport.

DOI: 10.1103/PhysRevLett.120.010501

Ion traps have been a workhorse in demonstrating many proof-of-principle experiments in quantum information processing using small ion samples [1]. A major challenge to transform this ansatz into a powerful quantum computing machine that can handle problems beyond the capabilities of classical super computers remains its scalability [2–5]. Error correction schemes allow us to fight the ever sooner death of fragile quantum information stored in larger and larger quantum systems, but their economic implementation requires computational building blocks to be executed with sufficient fidelity [6,7]. Essential computational steps have been demonstrated with fidelities beyond a threshold of 99.99% that is often considered as allowing for economic error correction [8] and, thus, for fault-tolerant scalable quantum information processing (QIP). These building blocks include single qubit rotation [9,10], individual addressing of interacting ions [11], and internal state detection [12]. In addition, high fidelity two-qubit quantum gates [10,13–16] and coherent three-qubit conditional quantum gates [17,18] have been implemented.

Straightforward scaling up to an arbitrary size of a single ion trap quantum register, at present, appears unlikely to be successful because the growing size of a single register usually introduces additional constraints imposed by the confining potential and by the Coulomb interaction of ion strings [19]. Even though, for instance, transverse modes and anharmonic trapping [20] may be employed for conditional quantum logic, a general claim might be that, at some point, it is useful to divide a single ion register into subsystems and to exchange quantum information between these subsystems [2–5]. One might do that by transferring quantum information from ions to photons (and vice versa) and by then exchanging photons between subsystems [4,21].

Alternatively, when exchanging quantum information between spatially separated individual registers within an ion trap-based quantum information processor, the transport of ions carrying this information is an attractive approach [2,3,5]. Methods to transport ions in segmented Paul traps have been developed and demonstrated [22–25], and optimized with respect to the preservation of the motional state during transport [26,27].

It is equally important to avoid errors of the quantum information encoded into internal states of ions during transport. Schemes relying on physical transport of ions require shuttling of ions between regions where the actual conditional gates take place (or between memory zones). Transport and single qubit manipulation can also be combined and executed at the same time [28].

Quantum error correction relies on the distribution of a logical qubit's information onto multiple qubits. Encoding and correction of this information consists, in general, of a number of single qubit rotations, entangling gates, measurements, and typically, either shuttling or spectroscopic decoupling of ions. To have the entire error correction sequence be beneficial, the constraints on the individual operations are obviously more stringent. For all correction schemes involving ion transport, the number of transport operations are bigger compared to or much larger than one [2,3,5,29], so the infidelity must, at least, be an order of magnitude smaller than acceptable for the entire sequence.

Therefore, in addition to high fidelity local gates, high fidelity transport is required to not cross a desired error threshold when carrying out single- and multiqubit quantum gates.

Several experiments have characterized the internal state fidelity $\mathcal{F} = \langle\psi|\rho|\psi\rangle$ upon transport by measuring the loss of coherence of a prepared superposition state $|\psi\rangle$ which dephases into a mixed state ρ during a Ramsey-type measurement. However, the precision reached in these experiments was not yet sufficient to conclude that transport takes place in the fault-tolerant regime required for scaling [22,24,26,27,30]. Here, we demonstrate high

fidelity transport of trapped ions over a distance of 280 μm with quantum information encoded into internal hyperfine states with a relative error of the qubit states per transport below 10^{-5} which is compatible with fault-tolerant and, thus, scalable quantum computation.

The determination of $\mathcal{F}$ is limited by the uncertainty of the extracted Ramsey-fringe contrast and the relative error is of the same order as the relative uncertainty of the contrast. In the experiments reported below, we determine the contrast of a Ramsey-type measurement typically with a relative error of $\leq 1 \times 10^{-2}$. Therefore, the straightforward extraction of fringe contrast from experimental data is not sufficient for precise determination of the error taking place during transport. To be able to precisely measure the loss of fidelity, we increase the number of transport operations M. To limit systematic errors due to a possible spatial variation of the qubit coherence time in the trap, we design the experiment such that the ions' average position is independent of M for $M > 0$ and compare the contrast after $M = 4000$ with the contrast obtained after $M = 2$ transport operations.

The ion trap is operated with singly charged ^{172}Yb and ^{171}Yb ions. ^{172}Yb^{+} ions possessing no hyperfine structure are employed to determine the efficiency of physical ion transport, while for the analysis of the transport induced decoherence, a hyperfine qubit in ^{171}Yb^{+} is used. As a qubit, we choose the first-order magnetic field insensitive hyperfine qubit composed of the states $|0\rangle \equiv |S_{1/2}, F = 0\rangle$ and $|1\rangle \equiv |S_{1/2}, F = 1, m_F = 0\rangle$. The second order magnetic field sensitivity of the qubit resonance frequency at $B = 640$ μT is $d\nu/dB = 39.7$ MHz/T. A detailed description of the laser and microwave setup can be found in [31].

The experiment is carried out in a 3D-Paul trap [32–35] divided into 33 segments, each consisting of two dc electrodes, and two global rf electrodes. In the experiments reported here, ions were transported by moving the minimum of the trapping potential from the center of one segment A to the center of the next segment B over a distance of 280 μm (see Fig. 1). The required potentials were generated by applying twelve voltage ramps to dc electrodes of six trap segments of the trap. One additional voltage ramp was applied to a correction electrode to allow for minimization of micromotion perpendicular to the dc electrodes' plane.

Methods to transport ions in segmented Paul traps have been investigated elaborately in a number of publications [22–24,27,36]. We use the approach worked out in Ref. [37] to calculate an optimized trajectory $\mathbf{r}(t)$ that minimizes ion heating during transport, an implementation of the boundary element method to simulate the potentials generated by our trap geometry [25], and the formalism described in Ref. [36] to calculate suitable transport voltages. To reduce limitations of the potential dynamics imposed by low pass filters of our dc electrodes, we extend this formalism by a method to constructively take into account the filter characteristics: Instead of trying to compensate the filter behavior after the transport voltage ramps $U(t)$ have been determined, we

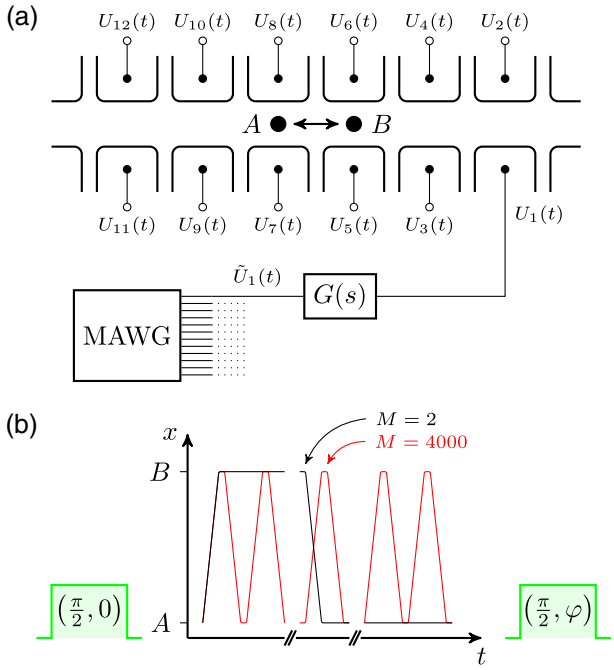

FIG. 1. Schematic of the experiment. (a) The voltages $\tilde{U}(t)$ at the multichannel arbitrary waveform generator (MAWG) take the filter characteristic $G(s)$ of the electronics into account to produce suitable voltages $U(t)$ that transport the ion along the x axis M times between positions A and B. (b) The timing of the transport operations is such that the ion is located equally long at A and B. The ion transfer is sandwiched by two $\pi/2$ pulses.

calculate the accessible voltage range for every point $\mathbf{r}_i = \mathbf{r}(t_i)$ during transport based on the voltage history $U(t_{k<i})$ and limit the potential optimization algorithm to this interval. Using this approach, we are able to realize single transport times of 12.8 μs on the order of the inverse filter cut off frequency (15.8 μs). See Supplemental Material (Section I) [38] for details.

In the experiment presented in this Letter, we performed 22×10^6 transport operations without losing an ion. The success of a single transport operation $A \rightarrow B$ or $B \rightarrow A$ is proven by imaging the ion fluorescence for a few milliseconds once the ion is at rest after transport. Because up to 2000 consecutive transport operations $A \rightarrow B \rightarrow A$ are investigated, the success of the overall transport (i.e., during M shuttling events) needs to be shown as well. Imaging the ion for several milliseconds at one position after every second transport operation would add seconds to every single repetition of the experiment, and, more importantly, change the transport dynamics by doppler-cooling of the ions. So to diagnose the success rate of consecutive transfers, we implemented an experiment to track the ion during M shuttling operations. During the transport operation the electron multiplying charge-coupled device camera takes one single image with an exposure time equal to the overall transport duration. Synchronized to the ion transport, we flash the detection laser at position A (B) for 2 μs each time the ion

should be at position B (A). The absence of the ion is signified by not detecting scattered resonance fluorescence. This experiment is not exactly tracking the ion, but it proves that it is not at a position where it should not be. We also perform measurements that flash the ion at position A (B) when it is expected to be there, but the statistics of these measurements are a factor 15 inferior compared to the more sensitive detection of an absent ion. This experiment is carried out using $^{172}Yb^{+}$, to profit from higher fluorescence rates. The analysis yields that $8(^{+12}_{-8})$ out of 4000 transport operations are failing. This number corresponds to a transport fidelity (the probability of transporting the ion as intended) of 99.8%. Combined with the ions presence after 22×10^6 transport operations, we interpret the obtained transport fidelity as a lower bound. See Supplemental Material (Section II) [38] for a detailed analysis of the transport fidelity.

The central goal of the Letter presented here is to determine the effect of ion transport operations on the qubit's internal state coherence. The internal state coherence is determined by performing a Ramsey-type experiment, where transport operations are executed during the free precession time: We initialize the qubit of a Doppler-cooled ion at position A in the $|0\rangle$ state. Using a microwave $\pi/2$ pulse, we prepare the superposition state $|\psi\rangle = 1/\sqrt{2}(|0\rangle - i|1\rangle)$. Next, the ion is transported M times between the positions A and B. We add waiting times at positions A and B such that the total precession time $t_p = 69.44$ ms is independent of M.

The waiting time is equally distributed between both positions. After a second $\pi/2$ pulse with a phase φ relative to the first pulse, the qubit state is read out.

We sample the Ramsey interference fringe for $M = 2$ and $M = 4000$ transport operations at 19 phase values φ. The Ramsey measurement for every setting is repeated 100 times (see Fig. 2).

We monitor fluorescence during Doppler-cooling and use a low fluorescence count (dark or absent ion) as a veto for the last and next Ramsey measurement (about 10% of the data). Besides electronic readout noise and background counts, the detection scheme is limited by off resonant excitation of the transitions $|S_{1/2}, F = 0\rangle - |P_{1/2}, F = 1\rangle$ and $|S_{1/2}, F = 1\rangle - |P_{1/2}, F = 1\rangle$ and following decay into $|S_{1/2}, F = 1\rangle$ resp. $|S_{1/2}, F = 0\rangle$. The former process results in the observation of fluorescence from a qubit originally in the $|0\rangle$ (dark) state, the latter one reduces the fluorescence of the $|1\rangle$ (bright) state. The same effect can be induced by spontaneous decay of the $|P_{1/2}, F = 0\rangle$ state to the $|D_{3/2}, F = 1\rangle$ state. By using two separate discrimination thresholds for dark and bright states in the data analysis, we can reduce the probability of wrongly identified states at the cost of reduced statistics [31,39].

For threshold selection, we add calibration runs to the experiment in which we omit the $\pi/2$ pulses but prepare the ion in the $|0\rangle$ ($|1\rangle$) state before the transport operations, to obtain detection histograms for pure $|0\rangle$ ($|1\rangle$) states. The $|1\rangle$ state is prepared by using a BB1RWR π pulse [40] that is robust against Rabi frequency errors. The calibration is done separately for both $M = 2$ and $M = 4000$ transport operations in order to account for possible variations of the detection statistics due to transport induced ion heating. Using these calibration measurements, we determine threshold values for state discrimination. In addition, the probabilities to correctly identify a bright state as bright $p_{\tilde{b}|b}$ and a dark state as dark $p_{\tilde{d}|d}$ can be extracted. We choose thresholds that yield $p_{\tilde{b}|b} = 0.964$ (0.959) and $p_{\tilde{d}|d} = 0.985$ (0.978) for $M = 4000$ ($M = 2$).

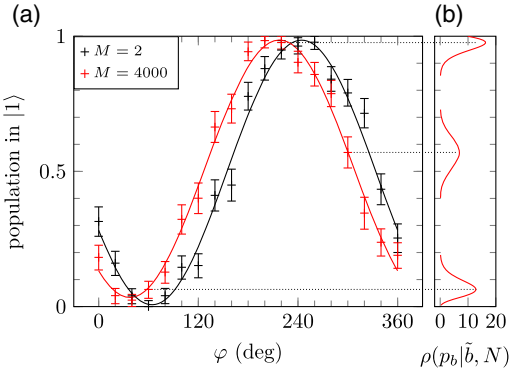

FIG. 2. (a) Ramsey fringes for 1 (black) and 4000 (red) ion transport operations. The relative phase φ between the two $\pi/2$ pulses is varied while the time between the pulses is kept constant. The decay of the amplitude due to the additional transport operations is hardly noticeable. (b) Three examples for the probability distributions that were used for the likelihood analysis of the data. The probability density $\rho(p_b|\tilde{b}, N)$ for $\tilde{b}$ bright events out of N trials is shown on the horizontal axis as a function of the probability p_b for a projection into the state $|1\rangle$ on the vertical axis.

The determination of coherence loss of the qubit state due to the transport operations is done by comparing the amplitudes of the obtained Ramsey fringes for different numbers of transport operations M. As we expect the infidelity to be close to zero, we need to employ several statistical methods to get precise results and error estimates. Since the efficiency of state selective detection is below unity, we distinguish between the actual number of projections b and d ($b, d \in \mathbb{N}_0$ and $b + d = N$) into states $|1\rangle$ and $|0\rangle$ and the corresponding numbers $\tilde{b}$ and $\tilde{d}$ identified as $|1\rangle$ and $|0\rangle$ during data analysis. To reconstruct the true fractional population of states $|0\rangle$ and $|1\rangle$ of a qubit state $|\psi\rangle$, we need to infer the numbers b and d from the numbers of identified states $\tilde{b}$ and $\tilde{d}$.

The obtained probability density $\rho(p_b|\tilde{b}, N)$ of the state population depends on the number of identified bright states, the number of measurements N, and the state identification probabilities $p_{\tilde{b}|b}$ and $p_{\tilde{d}|d}$.

The state population varies as a function of the relative phase of the second $\pi/2$ pulse and can be parametrized by

$$p_b(\varphi) = B + A \sin(\varphi - \Phi), \tag{1}$$

with the amplitude A, offset B, and phase shift Φ. We fit this model by maximizing the log likelihood

$$\log \mathcal{L}_M(A,B,\Phi) = \sum_{k=1}^{K} \log \rho(B + A\sin(\varphi_k - \Phi)|\tilde{b}_k, N_k), \tag{2}$$

for both numbers of transport operations M using the probability density function $\rho(p_b|\tilde{b},N)$ for the K data points $(\tilde{b}_k, N_k)$.

The coherence loss of our qubit in a static potential for precession times shorter than 100 ms is best described by a decay model $A(t) = \frac{1}{2}\exp(-\lambda t^2)$ for the amplitude A of the Ramsey fringe with $\lambda = 4(2)/s^2$. This corresponds to an expected amplitude of $A(t_p) = 0.490(5)$ of a Ramsey measurement without ion transport.

Figure 2(a) shows the Ramsey fringes obtained for $M = 2$ and $M = 4000$ transport operations. The error bars indicate the 68% confidence intervals of single data points. The right part, 2(b), displays the probability distribution $\rho(p_b|\tilde{b},N)$ for three exemplary data points. The amplitude of the $M = 4000$ curve is slightly reduced by 0.013 compared to $M = 2$, and the phase shift differs by 27°. We estimate the gradient of the magnetic field in the direction of the ion transport to be 10.6×10^{-3} T/m. This gradient results in a 120 Hz difference between the hyperfine splitting of the qubit at positions A and B. From simulations, we expect that the mean positions of the ions for 2 and 4000 transfers during the free precession time differ by 0.9 μm, due to nonperfect compensation of the dc electrode filters. This would correspond to a phase difference of 10°. The amplitude reduction observed with the number of transport operations is compatible with zero, in good agreement with our qubit being magnetic field insensitive to the first order. The Supplemental Material (Section III) [38] gives a short discussion of different sources for a possible decay.

The state identification probabilities $p_{\tilde{b}|b}$ and $p_{\tilde{d}|d}$ were treated up to this point as fixed error-free parameters. In reality, these values are calculated from a finite set of measurements and, therefore, bear additional uncertainties. We estimate these uncertainties by analyzing the calibration data obtained for state identification using the bootstrapping resampling method [41] and averaging the likelihoods $\mathcal{L}_M(A)$ over the results obtained for different choices of $p_{\tilde{b}|b}$ and $p_{\tilde{d}|d}$. See Supplemental Material (Section IV) [38] for details of the uncertainty estimation.

The likelihood distribution of the internal state fidelity during ion transport (Fig. 3) is calculated by a numerical convolution of the likelihoods of the Ramsey fringe amplitudes A_2 and A_{4000} according to

$$\mathcal{F} = \sqrt[4000-2]{\frac{A_2}{A_{4000}}}. \tag{3}$$

Here, we report a fidelity of the internal qubit state per transport operation of

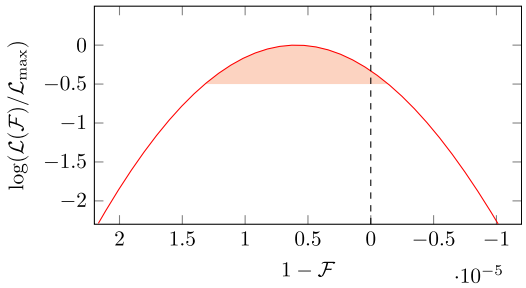

FIG. 3. Likelihood of the internal state fidelity $\mathcal{F}$ during ion transport. The loss of internal state fidelity due to the transfer of the ion is apparent, but the case of no loss of coherence is also compatible within the 68% confidence interval (shaded). The log likelihood is calculated by the numerical convolution of the likelihoods $\mathcal{L}_M$.

$$\mathcal{F} = 0.999\,994(^{+6}_{-7}). \tag{4}$$

This result is obtained under the assumption that each individual transport $A \to B$ and $B \to A$ out of a total of M attempted transports of an ion is actually successful, that is, the transport fidelity is perfect. Taking a finite probability of transport failure into account, the fidelity would change according to $\bar{\mathcal{F}}(M_f) = \mathcal{F}^{(4000-2)/(4000-2-M_f)}$, for M_f failing transports. The likelihood of $\mathcal{F}$ is almost Gaussian (compare Fig. 3), so we expect the error scaling of $\bar{\mathcal{F}}$ to follow $\sigma(\bar{\mathcal{F}}(M_f)) = [(4000-2)/(4000-2-M_f)]\mathcal{F}^{(M_f)/(4000-2-M_f)}\sigma(\mathcal{F})$. With the transport fidelity of 99.8% determined above, a 5σ deviation would result in $M_f = 68$ failed transports. This would reduce the internal state fidelity during ion transport by 1×10^{-7}, which is about an order of magnitude smaller than the statistical uncertainty of $\mathcal{F}$. A systematic error due to imperfect preparation of the $|0\rangle$ and $|1\rangle$ states also does not change the statistical significance of $\mathcal{F}$. See Supplemental Material (Section V) [38] for details of the error estimation.

In this Letter, we use the magnetic insensitive hyperfine qubit. Some schemes for QIP with trapped ions using radio-frequency and microwave radiation [42] utilize magnetic field dependent states, for example, the qubit composed of $|0\rangle$ and $|S_{1/2}, F = 1, m_F = \pm 1\rangle$. As the magnetic field sensitive qubit can be recoded into the insensitive qubit and back [18] the results of this Letter are also immediately relevant for these QIP schemes.

In summary, we demonstrate by precise measurements and careful data analysis that the physical transport of quantum information encoded in a hyperfine qubit can be carried out with a fidelity better than $1 - 10^{-5}$. This is an important prerequisite, together with high gate fidelities and low cross talk, for all schemes for scalable QIP with trapped ions that rely on the transport of ions.

We acknowledge funding from the European Community's Seventh Framework Programme under

Grant Agreement No. 270843 (Integrated Quantum Information Technology), from European Metrology Research Programme (EMRP) in Project No. SIB04 (the EMRP is jointly funded by the EMRP participating countries within the European Metrology Research Programme and the European Union).

*christof.wunderlich@uni-siegen.de;
http://quantenoptik.uni-siegen.de

[1] R. Blatt and D. Wineland, Nature (London) **453**, 1008 (2008).
[2] D. Kielpinski, C. Monroe, and D. J. Wineland, Nature (London) **417**, 709 (2002).
[3] K. M. Svore, A. V. Aho, A. W. Cross, I. Chuang, and I. L. Markov, *Computer* (IEEE Computer Society, 2006), Vol. 39, pp. 74–83.
[4] C. Monroe, R. Raussendorf, A. Ruthven, K. R. Brown, P. Maunz, L.-M. Duan, and J. Kim, Phys. Rev. A **89**, 022317 (2014).
[5] B. Lekitsch, S. Weidt, A. G. Fowler, K. Mølmer, S. J. Devitt, C. Wunderlich, and W. K. Hensinger, Sci. Adv. **3**, e1601540 (2017).
[6] P. W. Shor, Phys. Rev. A **52**, R2493 (1995).
[7] A. Steane, Proc. R. Soc. A **452**, 2551 (1996).
[8] E. Knill, Nature (London) **463**, 441 (2010).
[9] K. R. Brown, A. C. Wilson, Y. Colombe, C. Ospelkaus, A. M. Meier, E. Knill, D. Leibfried, and D. J. Wineland, Phys. Rev. A **84**, 030303 (2011).
[10] C. J. Ballance, T. P. Harty, N. M. Linke, M. A. Sepiol, and D. M. Lucas, Phys. Rev. Lett. **117**, 060504 (2016).
[11] C. Piltz, T. Sriarunothai, A. F. Varón Rojas, and C. Wunderlich, Nat. Commun. **5**, 4679 (2014).
[12] A. H. Burrell, D. J. Szwer, S. C. Webster, and D. M. Lucas, Phys. Rev. A **81**, 040302 (2010).
[13] J. Benhelm, G. Kirchmair, C. F. Roos, and R. Blatt, Nat. Phys. **4**, 463 (2008).
[14] T. P. Harty, M. A. Sepiol, D. T. C. Allcock, C. J. Ballance, J. E. Tarlton, and D. M. Lucas, Phys. Rev. Lett. **117**, 140501 (2016).
[15] J. P. Gaebler, T. R. Tan, Y. Lin, Y. Wan, R. Bowler, A. C. Keith, S. Glancy, K. Coakley, E. Knill, D. Leibfried, and D. J. Wineland, Phys. Rev. Lett. **117**, 060505 (2016).
[16] S. Weidt, J. Randall, S. C. Webster, K. Lake, A. E. Webb, I. Cohen, T. Navickas, B. Lekitsch, A. Retzker, and W. K. Hensinger, Phys. Rev. Lett. **117**, 220501 (2016).
[17] T. Monz, K. Kim, W. Hänsel, M. Riebe, A. S. Villar, P. Schindler, M. Chwalla, M. Hennrich, and R. Blatt, Phys. Rev. Lett. **102**, 040501 (2009).
[18] C. Piltz, T. Sriarunothai, S. S. Ivanov, S. Wölk, and C. Wunderlich, Sci. Adv. **2**, e1600093 (2016).
[19] M. Johanning, Appl. Phys. B **122**, 71 (2016).
[20] G.-D. Lin, S.-L. Zhu, R. Islam, K. Kim, M.-S. Chang, S. Korenblit, C. Monroe, and L.-M. Duan, Europhys. Lett. **86**, 60004 (2009).
[21] D. Hucul, I. V. Inlek, G. Vittorini, C. Crocker, S. Debnath, S. M. Clark, and C. Monroe, Nat. Phys. **11**, 37 (2015).
[22] M. A. Rowe, A. Ben-Kish, B. Demarco, D. Leibfried, V. Meyer, J. Beall, J. Britton, J. Hughes, W. M. Itano, B. Jelenković, C. Langer, T. Rosenband, and D. J. Wineland, Quantum Inf. Comput. **2**, 257 (2002).
[23] W. K. Hensinger, S. Olmschenk, D. Stick, D. Hucul, M. Yeo, M. Acton, L. Deslauriers, C. Monroe, and J. Rabchuk, Appl. Phys. Lett. **88**, 034101 (2006).
[24] R. B. Blakestad, C. Ospelkaus, A. P. VanDevender, J. M. Amini, J. Britton, D. Leibfried, and D. J. Wineland, Phys. Rev. Lett. **102**, 153002 (2009).
[25] K. Singer, U. Poschinger, M. Murphy, P. Ivanov, F. Ziesel, T. Calarco, and F. Schmidt-Kaler, Rev. Mod. Phys. **82**, 2609 (2010).
[26] R. Bowler, J. Gaebler, Y. Lin, T. R. Tan, D. Hanneke, J. D. Jost, J. P. Home, D. Leibfried, and D. J. Wineland, Phys. Rev. Lett. **109**, 080502 (2012).
[27] A. Walther, F. Ziesel, T. Ruster, S. T. Dawkins, K. Ott, M. Hettrich, K. Singer, F. Schmidt-Kaler, and U. Poschinger, Phys. Rev. Lett. **109**, 080501 (2012).
[28] L. E. de Clercq, H.-Y. Lo, M. Marinelli, D. Nadlinger, R. Oswald, V. Negnevitsky, D. Kienzler, B. Keitch, and J. P. Home, Phys. Rev. Lett. **116**, 080502 (2016).
[29] J. Chiaverini, R. B. Blakestad, J. Britton, J. D. Jost, C. Langer, D. Leibfried, R. Ozeri, and D. J. Wineland, Quantum Inf. Comput. **5**, 419 (2005).
[30] We assume Gaussian errors of the reported Ramsey fringe contrasts and calculate the fidelity as $\mathcal{F} = \sqrt[M]{C_M/C_0}$), where C_0 is the contrast before and C_M after M transport operations.
[31] N. V. Vitanov, T. F. Gloger, P. Kaufmann, D. Kaufmann, T. Collath, M. Tanveer Baig, M. Johanning, and C. Wunderlich, Phys. Rev. A **91**, 033406 (2015).
[32] D. Kaufmann, T. Collath, M. T. Baig, P. Kaufmann, E. Asenwar, M. Johanning, and C. Wunderlich, Appl. Phys. B **107**, 935 (2012).
[33] S. Schulz, U. Poschinger, K. Singer, and F. Schmidt-Kaler, Fortschr. Phys. **54**, 648 (2006).
[34] S. A. Schulz, U. Poschinger, F. Ziesel, and F. Schmidt-Kaler, New J. Phys. **10**, 045007 (2008).
[35] M. T. Baig, M. Johanning, A. Wiese, S. Heidbrink, M. Ziolkowski, and C. Wunderlich, Rev. Sci. Instrum. **84**, 124701 (2013).
[36] R. B. Blakestad, C. Ospelkaus, A. P. VanDevender, J. H. Wesenberg, M. J. Biercuk, D. Leibfried, and D. J. Wineland, Phys. Rev. A **84**, 032314 (2011).
[37] E. Torrontegui, S. Ibáñez, X. Chen, A. Ruschhaupt, D. Guéry-Odelin, and J. G. Muga, Phys. Rev. A **83**, 013415 (2011).
[38] See Supplemental Material at http://link.aps.org/supplemental/10.1103/PhysRevLett.120.010501 for details of the transport potential calculations, the verification of consecutive ion transport, a discussion of possible sources of qubit dephasing, and details of the statistical and systematical error estimations.
[39] S. Wölk, C. Piltz, T. Sriarunothai, and C. Wunderlich, J. Phys. B **48**, 075101 (2015).
[40] H. K. Cummins, G. Llewellyn, and J. A. Jones, Phys. Rev. A **67**, 042308 (2003).
[41] B. Efron and R. Tibshirani, *An Introduction to the Bootstrap* (Taylor & Francis, London, 1994).
[42] F. Mintert and C. Wunderlich, Phys. Rev. Lett. **87**, 257904 (2001).